

## **Electronic supplementary information for:**

**Evidence for an egg-box-like structure in iron(II)-polygalacturonate hydrogels: a combined EXAFS and molecular dynamics simulation study**

Aline Maire du Poset,<sup>a,b,c</sup> Andrea Zitolo,<sup>\*b</sup> Fabrice Cousin,<sup>c</sup> Ali Assifaoui<sup>a</sup> and Adrien Lerbret<sup>\*a</sup>

<sup>a</sup>Univ. Bourgogne Franche-Comté, AgroSup Dijon, PAM UMR A 02.102, F-21000 Dijon, France.

<sup>b</sup>Synchrotron SOLEIL, L'Orme des Merisiers, BP 48 St Aubin, 91192 Gif-sur-Yvette, France.

<sup>c</sup>Laboratoire Léon Brillouin, Université Paris-Saclay, CEA-Saclay, 91191 Gif-sur-Yvette, France.

## EXAFS analysis of the Fe<sup>2+</sup>-polyGalA hydrogel

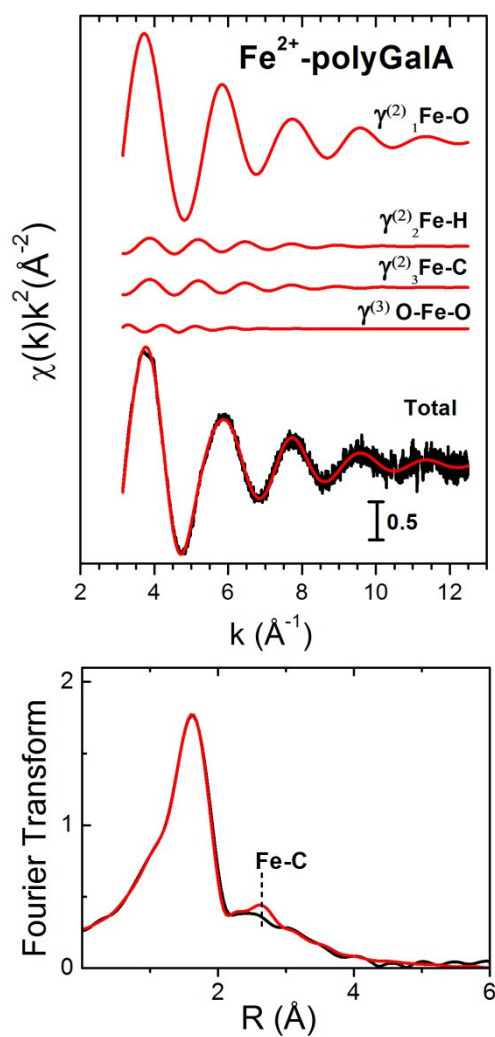


Figure S1. Fe K-edge EXAFS analysis of the Fe<sup>2+</sup>-polyGalA hydrogel via the GNXAS program. Upper panel: Fe-O, Fe-H, Fe-C  $\gamma^{(2)}$  two-body signals, and the O-Fe-O  $\gamma^{(3)}$  three-body signal included in the fit, the total signal (red line) superimposed to the experimental one (black line). Lower panel: the fit in the Fourier transformed space.

## XANES spectra of Fe<sup>2+</sup> in aqueous solution and in the Fe<sup>2+</sup>-polyGalA hydrogel

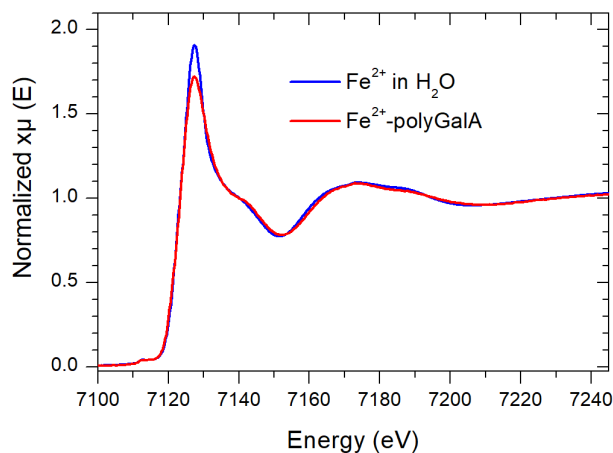


Figure S2. Fe K-edge XANES experimental spectra of a 0.1 M Fe<sup>2+</sup> water solution (blue curve) and of the Fe<sup>2+</sup>-polyGalA hydrogel (red curve).

## Fe<sup>2+</sup>-O distance from the literature

Table S1. Fe-O distance for Fe<sup>2+</sup> aqueous solutions determined from various experimental - EXAFS (Extended X-Ray Absorption Fine Structure), XRD (X-ray diffraction), ND (Neutron diffraction) - and numerical - MC (Monte Carlo), MD (Molecular dynamics), QMCF-MD (Quantum mechanical charge field molecular dynamics), QM/MM (Quantum mechanical/molecular mechanical) - studies from the literature.

Method	R(Fe-O) (Å)
EXAFS	2.095 <sup>1</sup> , 2.10 ± 0.01 <sup>2</sup> , 2.10 <sup>3</sup> , 2.10 (R <sub>m</sub> =2.12) <sup>4</sup> , 2.11 ± 0.01 (this work)
XRD	2.12 <sup>5</sup> , 2.24/2.28 <sup>6</sup> ,
ND	2.13 <sup>7</sup>
MC	2.10 <sup>8</sup>
MD	2.075 ± 0.025 <sup>9</sup> , 2.08 <sup>10</sup> , 2.09 <sup>11,12</sup> , 2.11 <sup>13,14</sup> , 2.113 <sup>15</sup> , 2.12 <sup>16</sup> , 2.13 ± 0.04 <sup>17</sup> , 2.15 <sup>18,19</sup>
QMCF-MD	2.15 <sup>20</sup>
QM/MM	2.10 <sup>21</sup>

## Molecular dynamics simulations

### Fe<sup>2+</sup> empirical potentials

Many efforts have been performed to develop reliable, non-polarizable empirical models of Fe<sup>2+</sup> and various strategies have been followed.<sup>10,13-17,22</sup> Both bonded<sup>23</sup>, non-bonded point charge<sup>10,13,14</sup>, and cationic dummy atom models<sup>15,17</sup> were designed. Bonded models are not suitable for the purpose of our study, since they do not allow ligand exchanges. In this work, we considered three non-bonded point charge models and two dummy models from the literature : (1) the 12-6 Lennard-Jones nonbonded model of Babu and Lim<sup>10</sup>, (2) the 12-6-4 nonbonded model of Li and Merz<sup>14</sup>, (3) the empirical potential developed by Curtiss et al.<sup>13</sup>, (4) the dummy model of Duarte et al.<sup>17</sup> and (5) the dummy model of Jiang et al.<sup>15</sup>.

Nonbonded interactions between atoms *i* and *j* separated by a distance  $r_{ij}$  are described by a sum of electrostatic and van der Waals interaction potentials:

$$U_{ij}(r_{ij}) = U_{elec,ij}(r_{ij}) + U_{vdw,ij}(r_{ij})$$

The electrostatic potential is :

$$U_{elec,ij}(r_{ij}) = \frac{1}{4\pi\epsilon_0} \frac{q_i \cdot q_j}{r_{ij}}$$

where  $q_i$  and  $q_j$  are the charges on atoms *i* and *j*, respectively, and  $\epsilon_0$  is the vacuum permittivity.

van der Waals interactions,  $U_{vdw,ij}$ , are represented by various potentials, as described below :

- 12-6 Lennard-Jones potential for the 12-6 and Dummy Jiang models:

$$U_{vdw,ij}(r_{ij}) = \epsilon_{ij} \left[ \left( \frac{R_{min,ij}}{r_{ij}} \right)^{12} - 2 \cdot \left( \frac{R_{min,ij}}{r_{ij}} \right)^6 \right]$$

where  $r_{ij}$  is the distance separating atoms *i* and *j*,  $\epsilon_{ij}$  is the energy well depth, and  $R_{min,ij}$  is the distance at the energy minimum for atoms *i* and *j*.

- 12-6 Lennard-Jones potential for the Dummy model :

$$U_{vdw,ij}(r_{ij}) = \frac{A_{ij}}{r_{ij}^{12}} - \frac{B_{ij}}{r_{ij}^6}$$

where  $A_{ij}$  and  $B_{ij}$  are the geometric Lennard-Jones parameters for the interaction between atoms *i* and *j*.  $A_{ij}$  and  $B_{ij}$  parameters are defined per atom type as  $A_i$  and  $B_i$  and are combined using the geometric rule:  $A_{ij} = A_i A_j$  and  $B_{ij} = B_i B_j$ , where  $A_i = A_{ii}^{1/2}$  and  $B_i = B_{ii}^{1/2}$ . Note that this form is equivalent to the standard one:

$$U_{vdw,ij}(r_{ij}) = 4 \cdot \epsilon_{ij} \left[ \left( \frac{\sigma_{ij}}{r_{ij}} \right)^{12} - \left( \frac{\sigma_{ij}}{r_{ij}} \right)^6 \right],$$

with:  $A_{ij} = 4\epsilon_{ij}\sigma_{ij}^{12}$  and  $B_{ij} = 4\epsilon_{ij}\sigma_{ij}^6$ , that is,  $\sigma_{ij} = (A_{ij}/B_{ij})^{1/6}$  and  $\epsilon_{ij} = B_{ij}^2/(4A_{ij})$ . Nevertheless,  $\epsilon_{ij}$  and  $\sigma_{ij}$  cannot be determined from  $A_{ij}$  and  $B_{ij}$  for dummy atoms, D, in the model of Duarte et al., because B is 0.

- 12-6-4 Lennard-Jones potential for the 12-6-4 model:

$$U_{vdw,ij}(r_{ij}) = \epsilon_{ij} \left[ \left( \frac{R_{min,ij}}{r_{ij}} \right)^{12} - 2 \cdot \left( \frac{R_{min,ij}}{r_{ij}} \right)^6 \right] - \frac{C_4^{ij}}{r_{ij}^4}$$

where the  $C_4^{ij}/r_{ij}^4$  term accounts for ion-induced dipole interactions.

- Curtiss dispersion potential:

$$U_{vdw,Fe-O}(r_{Fe-O}) = A \cdot \exp(-B \cdot r_{Fe-O}) - \frac{D}{r_{Fe-O}^6} - \frac{E}{r_{Fe-O}^8} - \frac{F}{r_{Fe-O}^{12}}$$

where A, B, D, E, and F are potential parameters. The model of Curtiss *et al.* represents Fe<sup>2+</sup>-water interactions with a non-standard dispersion potential, so that Lorentz-Berthelot or geometric mixing rules cannot be used to determine parameters for Fe-GalA interactions. To overcome this problem, Fe-GalA interactions were calculated with other Fe<sup>2+</sup> models (either 12-6 or 12-6-4).

The non-bonded parameters of all investigated Fe<sup>2+</sup> potentials are summarized in Table S2. Further details may be found in the corresponding references.

**Table S2. Simulation parameters for the various Fe<sup>2+</sup> models considered in this study.**

Model type	Fe <sup>2+</sup> model	Atom	Mass (g.mol <sup>-1</sup> )	Charge (e)	Non-bonded parameters*
Point charge	12-6 <sup>10</sup>	Fe	55.845	+2.0	R <sub>min</sub> /2 = 1.3488 Å; ε = 0.0264 kcal.mol <sup>-1</sup>
	12-6-4 <sup>14</sup>	Fe	55.845	+2.0	R <sub>min</sub> /2 = 1.457 Å; ε = 0.02710805 kcal.mol <sup>-1</sup> C <sub>4</sub> = 163.0 Å <sup>4</sup> .kcal.mol <sup>-1</sup>
	Curtiss <sup>13</sup>	Fe	55.845	+2.0	A=24.33 Ha; B=1.735 Bohr <sup>-1</sup> ; D=21.73 Ha.Bohr <sup>6</sup> E=43.25 Ha.Bohr <sup>8</sup> ; F=-878.14 Ha.Bohr <sup>12</sup>
Dummy	Duarte <sup>17</sup>	Fe	37.85	-1.0	A=70.0 kcal <sup>1/2</sup> .mol <sup>-1/2</sup> .Å <sup>-6</sup> B=10.0 kcal <sup>1/2</sup> .mol <sup>-1/2</sup> .Å <sup>-3</sup>
		D	3.0	+0.5	A=0.05 kcal <sup>1/2</sup> .mol <sup>-1/2</sup> .Å <sup>-6</sup> B=0.00 kcal <sup>1/2</sup> .mol <sup>-1/2</sup> .Å <sup>-3</sup>
	Jiang <sup>15</sup>	Fe	37.85	-1.0	R <sub>min</sub> /2 = 0.6857 Å; ε = 9.6775 kcal.mol <sup>-1</sup>
		D	3.0	+0.5	R <sub>min</sub> /2 = 1.3882 Å; ε = 10 <sup>-8</sup> kcal.mol <sup>-1</sup>

\*1 Ha ≈ 627.509 kcal.mol<sup>-1</sup>; 1 Bohr ≈ 0.529 Å

Figure S3 shows the Fe<sup>2+</sup>-TIP3P H<sub>2</sub>O interaction potential for the various models of Fe<sup>2+</sup> considered as a function of the Fe<sup>2+</sup>-water oxygen distance, r. The distance, r<sub>min</sub>, and interaction energy of the minimum, E<sub>min</sub>, as well as the associated effective spring constant, k<sub>eff</sub>, are given in Table S3. Significant differences are observed among the interaction potentials, particularly between the Curtiss model and the other ones. Differences as large as 0.2 Å are obtained for r<sub>min</sub> between the Curtiss and the Dummy model. Similarly, E<sub>min</sub> ranges between -278.0 and -232.3 kJ.mol<sup>-1</sup> and k<sub>eff</sub> is more than 5 times smaller for the Curtiss model than for the Dummy Jiang one.

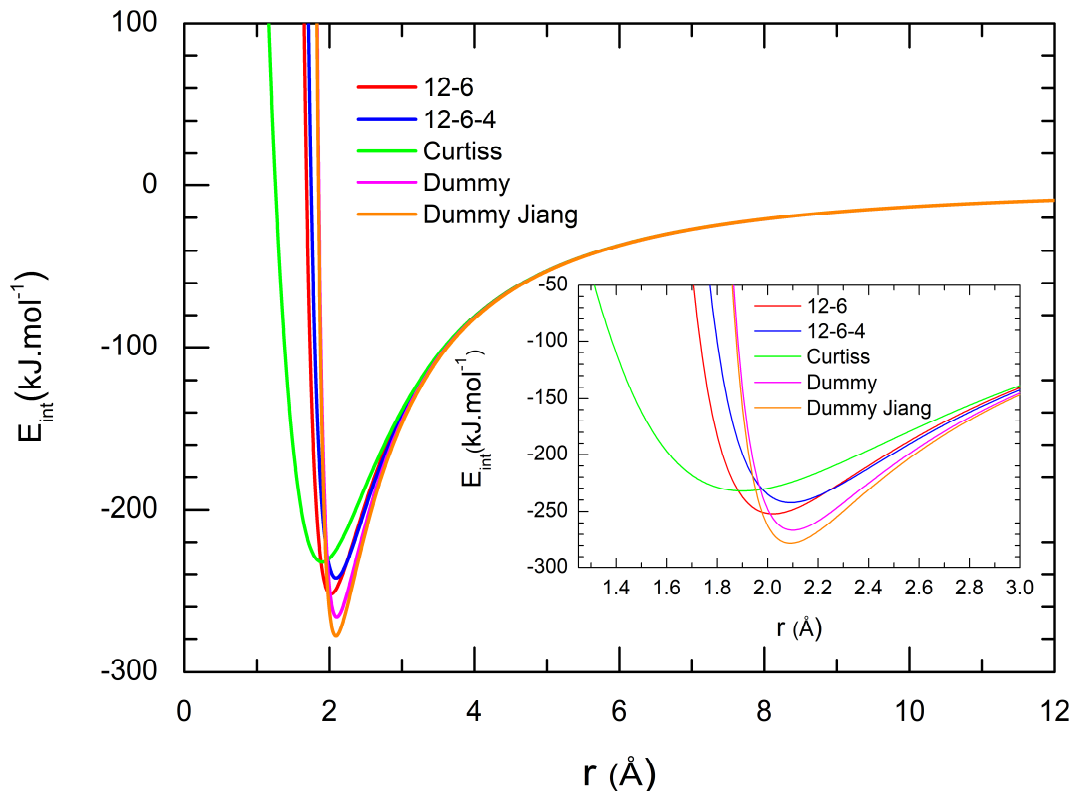


**Figure S3.**  $\text{Fe}^{2+}$ -TIP3P water interaction potential as a function of the  $\text{Fe}^{2+}$ -water oxygen distance,  $r$ , for the various  $\text{Fe}^{2+}$  models considered in this study. The inset shows a zoom on the minimum region of these potentials to better visualize differences in the minimum position and in the curvatures of these potentials.

**Table S3.**  $\text{Fe}^{2+}$ -water oxygen distance,  $r_{\text{min}}$ , and value,  $E_{\text{min}}$ , of the minimum of the  $\text{Fe}^{2+}$ -TIP3P  $\text{H}_2\text{O}$  interaction potential for the various  $\text{Fe}^{2+}$  models considered in this study. The corresponding effective spring constant,  $k_{\text{eff}}$ , is also provided.  $k_{\text{eff}}$  was obtained by fitting the interaction potentials,  $E_{\text{int}}(r)$ , against  $1/2 * k_{\text{eff}} * (r - r_{\text{min}})^2 + E_{\text{min}}$  on the  $[r_{\text{min}} - \delta; r_{\text{min}} + \delta]$  interval ( $\delta$  was set to 0.05 Å).

$\text{Fe}^{2+}$ model	$r_{\text{min}}$ (Å)	$E_{\text{min}}$ (kJ.mol <sup>-1</sup> )	$k_{\text{eff}}$ (kJ.mol <sup>-1</sup> .Å <sup>-2</sup> )
12-6	2.02	-252.1	1431
12-6-4	2.09	-242.3	1338
Curtiss	1.90	-232.3	463
Dummy	2.10	-266.4	2394
Dummy Jiang	2.09	-278.0	2651

### Comparison of $\text{Fe}^{2+}$ models

Three geometrical parameters were determined to compare the various  $\text{Fe}^{2+}$  models : (1) the ion-oxygen distance (IOD),  $d_{\text{Fe-O}}$ , and the average ion-oxygen distance,  $\bar{d}_{\text{Fe-O}}$ , (2) the coordination number of iron, CN, and (3) the average octahedral order parameter,  $\bar{q}_{\text{oct}}$ <sup>24,25</sup>.  $d_{\text{Fe-O}}$  was determined by fitting the first peak of the Fe-O radial distribution function,  $g(r)$ , with a gaussian function.  $\bar{d}_{\text{Fe-O}}$  was calculated for all oxygen atoms located at a distance below the position of the first minimum of the Fe-O  $g(r)$ ,  $r_{\text{m}}$ . CN was determined from the integral of  $g(r)$  up to  $r_{\text{m}}$ :

$$\text{CN} = \int_0^{r_{\text{m}}} 4\pi \cdot r^2 \cdot g(r) \cdot \rho \cdot dr$$

where  $\rho$  is the average density.

$\bar{q}_{\text{oct}}$  was determined as follows:

$$q_{\text{oct}} = \frac{1}{90} \times \sum_{j \neq k}^{N_n} 3 \cdot H(\theta_k - \theta_{\text{thr}}) \cdot \exp \left[ -\frac{1}{2} \left( \frac{\theta_k - \pi}{\Delta\theta_1} \right)^2 \right] \\ + \sum_{m \neq j, k}^{N_n} H(\theta_{\text{thr}} - \theta_k) \cdot H(\theta_{\text{thr}} - \theta_m) \cdot \cos^2(2\varphi) \cdot \exp \left[ -\frac{1}{2} \left( \frac{\theta_m - \pi/2}{\Delta\theta_2} \right)^2 \right]$$

where  $H(x)$  denotes the Heaviside function, which is 1 for  $x > 0$  and is 0 otherwise.  $\theta_k$  is the polar angle formed between the bonds of neighboring atoms  $j$  and  $k$  with their mutually bonded atom  $i$ ,  $\varphi$  is the azimuth angle between bond  $i$ - $m$  with the plane spanned by atoms  $i$ ,  $j$ , and  $k$ , and  $\Delta\theta_i$  ( $i=1,2$ ) are parameters controlling the reward loss for increasingly non-ideal positions.  $\theta_{\text{thr}}$  is a threshold angle to distinguish second neighbors that are considered to be either in a « South pole » configuration or in a « prime meridian » position.  $\theta_{\text{thr}}$ ,  $\Delta\theta_1$ , and  $\Delta\theta_2$  were set to  $8/9\pi$ ,  $\pi/15$  and  $\pi/18$ , respectively. Only the six nearest oxygen atoms from  $\text{Fe}^{2+}$  were considered ( $N_n=6$ ). Further details on the calculation of  $q_{\text{oct}}$  may be found in ref. [24,25].

### *Influence of water models*

Because the investigated structural parameters ( $d_{\text{Fe-O}}$ ,  $\bar{d}_{\text{Fe-O}}$ , CN, and  $\bar{q}_{\text{oct}}$ ) may depend both on the  $\text{Fe}^{2+}$  and on the water models, several water potentials other than TIP3P<sup>26</sup> were combined with the five  $\text{Fe}^{2+}$  models considered in this study: SPC,<sup>27</sup> SPC/E,<sup>28</sup> TIP4P-Ew.<sup>29</sup> For each pair of  $\text{Fe}^{2+}$  and water models, two systems were simulated to assess the quality of the considered empirical potentials: (i) a  $\text{Fe}^{2+}$  cation in the presence of two chloride anions (for electroneutrality of the simulation box) solvated by 1000 water molecules, and (ii) two octameric chains of polyGalA bridged by 4  $\text{Fe}^{2+}$  in the presence of 8 sodium cations (for electroneutrality of the simulation box) solvated by 3600 water molecules. This second system corresponds to an association of polyGalA in the egg-box model configuration and was previously simulated to compare  $\text{Ca}^{2+}$  and  $\text{Zn}^{2+}$  (see Fig. 4 of ref. [30]). The results for all simulated systems are summarized in Table S4. They show that the influence of the water model on the structure of the first coordination shell of  $\text{Fe}^{2+}$  is rather limited. Thus, only the TIP3P water potential<sup>31</sup> modified for the CHARMM force field<sup>26</sup> was used in this work, since the CHARMM36 force field<sup>32-34</sup> that represents GalA was parameterized with this water model.

**Table S4. Comparison of geometrical parameters (iron-oxygen distance: (i) peak position of Fe-O  $g(r)$ ,  $d_{\text{Fe-O}}$  (Å), and (ii) average value,  $\bar{d}_{\text{Fe-O}}$ , coordination number of iron, CN, and average octahedral order parameter,  $\bar{q}_{\text{oct}}$ ) for iron in water and for iron complexed with two polyGalA octamers obtained with different iron and water force fields. For the 12-6 and Dummy Jiang models of  $\text{Fe}^{2+}$ , the Fe-O  $g(r)$  for  $\text{Fe}^{2+}$  complexed with polyGalA exhibits two peaks, so that two values are provided for  $d_{\text{Fe-O}}$ .**

Force field		Simulated system							
		Fe <sup>2+</sup> in aqueous solution				Fe <sup>2+</sup> complexed to GalA chains			
Iron	Water	$d_{\text{Fe-O}}$ (Å)	$\bar{d}_{\text{Fe-O}}$ (Å)	CN	$\bar{q}_{\text{oct}}$	$d_{\text{Fe-O}}$ (Å)	$\bar{d}_{\text{Fe-O}}$ (Å)	CN	$\bar{q}_{\text{oct}}$
12-6	TIP3P	2.08	2.10 ± 0.06	6.00	0.81	1.95/2.10**	2.09 ± 0.12	6.00	0.76
	SPC/E	2.09	2.11 ± 0.06	6.00	0.82	1.96/2.10**	2.09 ± 0.11	6.00	0.77
12-6-4	TIP3P	2.10	2.11 ± 0.05	6.02	0.78	2.12	2.13 ± 0.08	6.70	0.49
	SPC/E	2.10	2.11 ± 0.05	6.00	0.82	2.10	2.11 ± 0.09	6.29	0.64
	TIP4P-Ew	2.10	2.11 ± 0.05	6.00	0.81	2.11	2.12 ± 0.08	6.75	0.45
Dummy	TIP3P	2.12	2.13 ± 0.04	6.00	0.82	2.12	2.13 ± 0.05	6.00	0.77
	SPC	2.13	2.14 ± 0.04	6.00	0.83	2.13	2.14 ± 0.06	6.00	0.74
Dummy Jiang	TIP3P	2.11	2.12 ± 0.04	6.00	0.83	2.03/2.11**	2.10 ± 0.07	6.01	0.74
	SPC/E	2.11	2.11 ± 0.04	6.00	0.84	2.02/2.11**	2.10 ± 0.08	6.00	0.77
	TIP4P-Ew	2.11	2.11 ± 0.04	6.00	0.83	2.00/2.12**	2.09 ± 0.08	6.00	0.78
Curtiss/12-6-4	TIP3P	2.08	2.11 ± 0.10	6.00	0.78	2.10	2.18 ± 0.11	6.97	0.27
	SPC	2.09	2.12 ± 0.10	6.00	0.79	2.10	2.17 ± 0.11	6.97	0.28
	SPC/E	2.08	2.11 ± 0.10	6.00	0.80	2.10	2.17 ± 0.11	6.98	0.27
	TIP4P-Ew	2.10	2.13 ± 0.10	6.00	0.78	2.08	2.18 ± 0.14	6.93	0.27
Curtiss/12-6	TIP3P	-	-	-	-	2.07	2.14 ± 0.14	6.81	0.33
	SPC	-	-	-	-	2.06	2.13 ± 0.15	6.47	0.21

\*\* Positions of the two peaks of the bimodal distribution.

## Comparison between experimental EXAFS spectra and theoretical signals determined from MD simulations

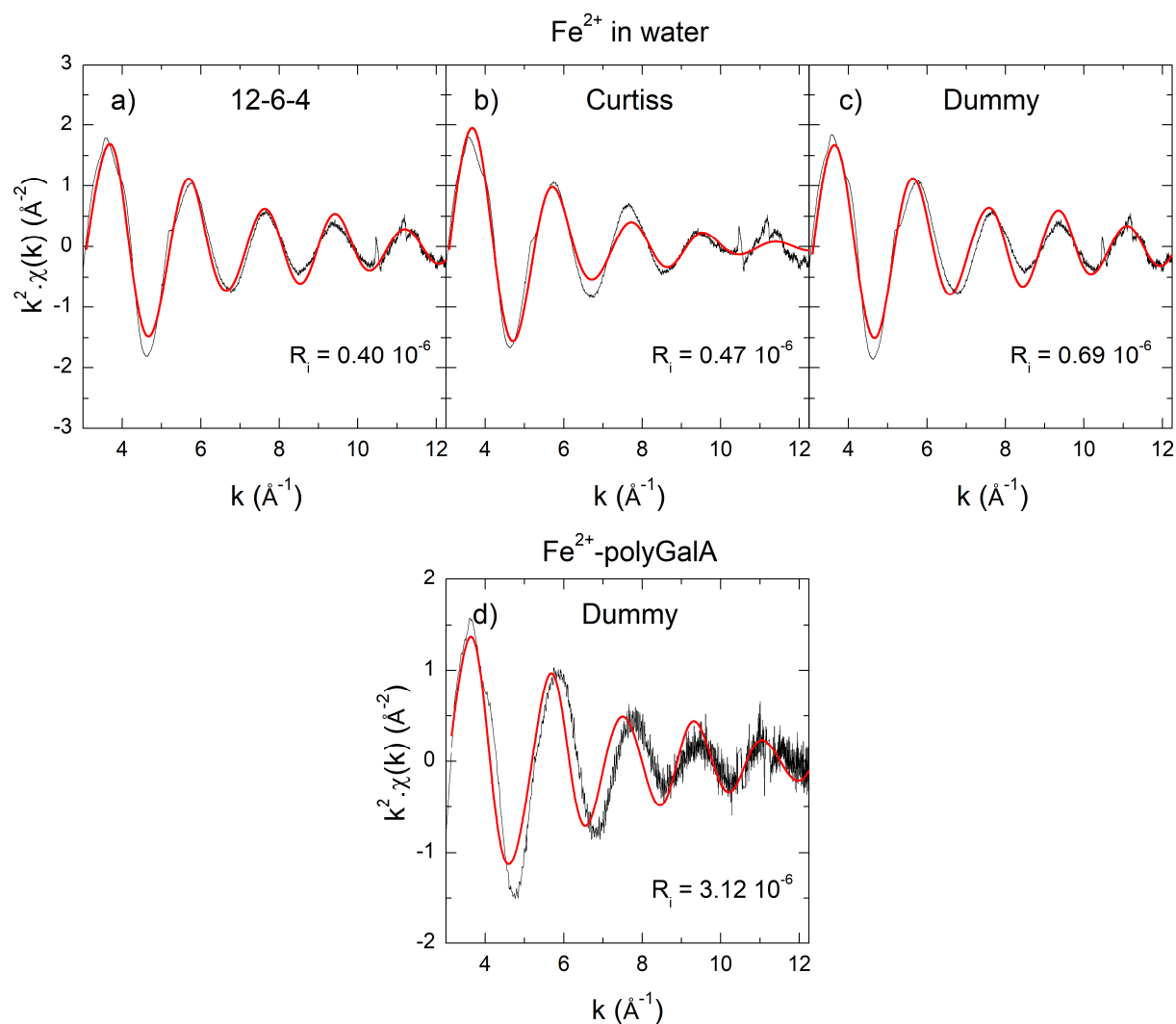
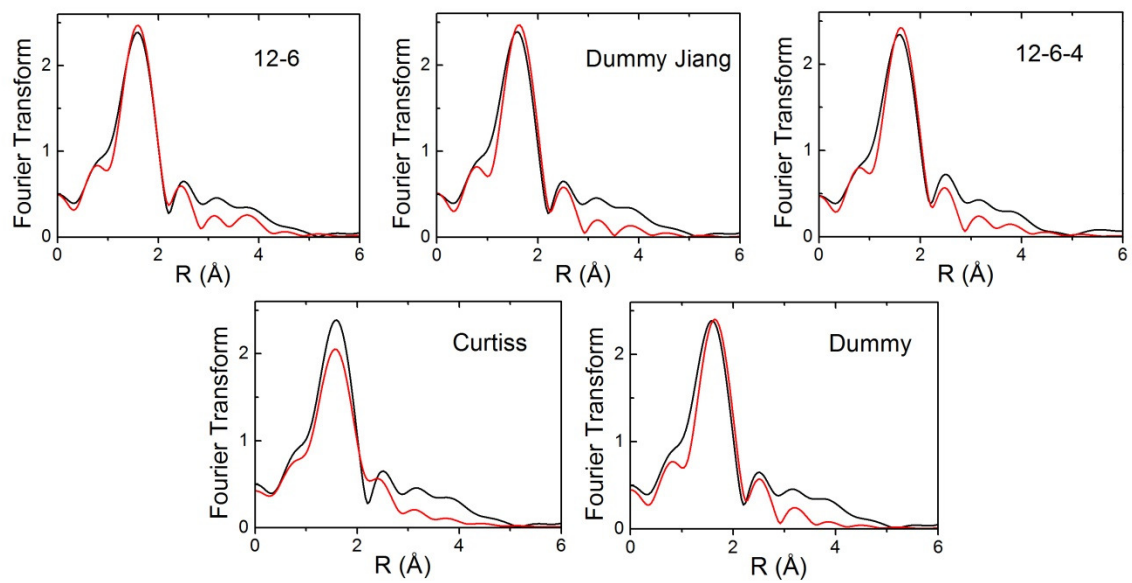


Figure S4. Comparison between the EXAFS experimental spectra (black lines) and the theoretical signals determined from Fe-O and Fe-H  $g(r)$  (red lines):  $\text{Fe}^{2+}$  in water with the (a) 12-6-4, (b) Curtiss, and (c) Dummy models;  $\text{Fe}^{2+}$  complexed with polyGalA with the Dummy model (d). EXAFS theoretical signals for  $\text{Fe}^{2+}$  complexed with polyGalA obtained with the 12-6-4, Curtiss/12-6, and Curtiss/12-6-4 models are not shown, given that they strongly overestimate the CN of  $\text{Fe}^{2+}$  (see Table 2).



**Figure S5. Comparison between the Fourier transform of the EXAFS experimental spectrum of  $\text{Fe}^{2+}$  in water solution (black lines) and of the theoretical signals determined from MD simulations (red lines).**

## Decomposition of $\text{Fe}^{2+}\text{-O } g(r)$

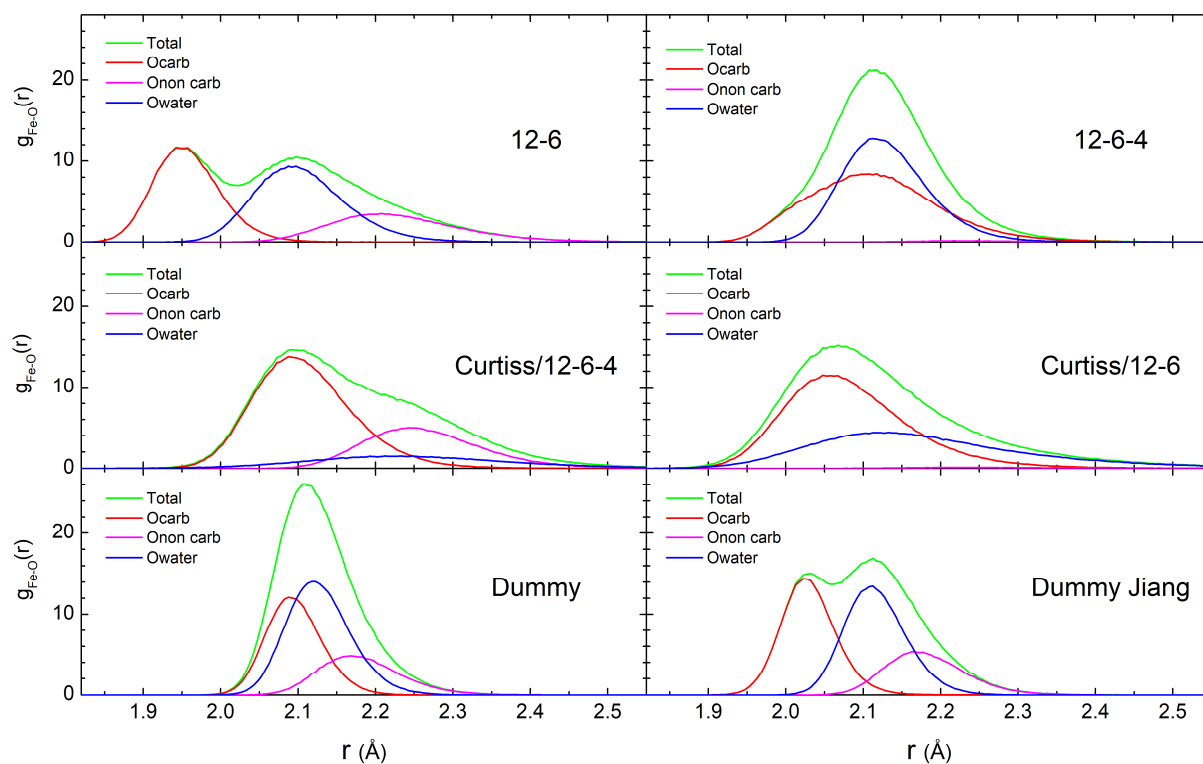
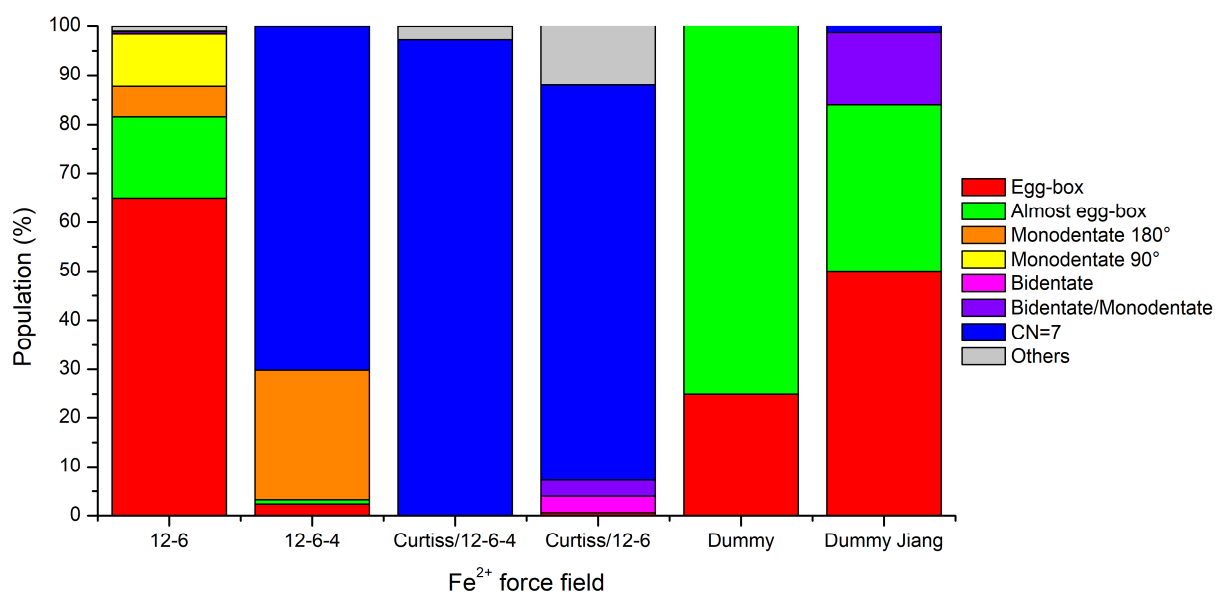


Figure S6. Fe-O  $g(r)$  for  $\text{Fe}^{2+}$  complexed with two polyGalA chains and decomposition into contributions from carboxylate (Ocarb), non-carboxylate (Onon carb), and water oxygen atoms (Owater) for the various  $\text{Fe}^{2+}$  force fields considered in this study.

## Distributions of coordination modes sampled with the various Fe<sup>2+</sup> models



**Figure S7.** Percentage probability distribution of the local coordination geometries of Fe<sup>2+</sup> sampled in the simulations of two octameric GalA chains in the antiparallel arrangement in the presence of four Fe<sup>2+</sup> cations represented with the different Fe<sup>2+</sup> force fields considered in this study. Configurations with a CN of 7 were also considered, while those with a CN of 5 or 8 were neglected, since they contribute respectively to at most 0.1 % and 0.02 % of the total of sampled configurations for a given force field. Configurations with a CN of 6 not described by the model coordination geometries considered in this study are referred to as “Others”. Note that no SSIP or monocomplexation coordination was sampled.

**Comparison between the Fourier transform of the experimental EXAFS spectrum of Fe<sup>2+</sup> in the polyGalA hydrogel and the theoretical signals determined from the restrained MD simulations of model coordination modes**

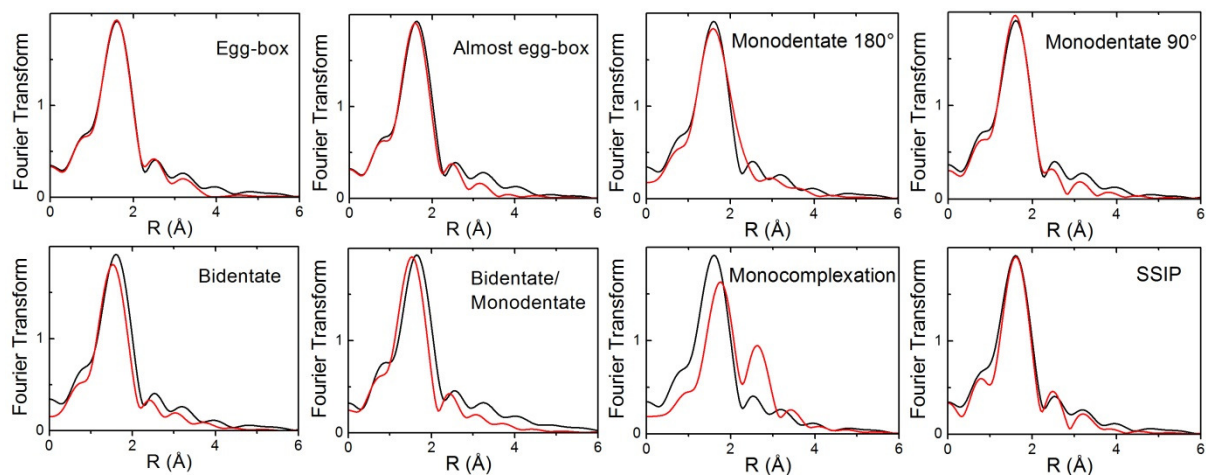


**Figure S8. Comparison between the Fourier transform of the EXAFS experimental spectra of Fe<sup>2+</sup> in the polyGalA hydrogel (black lines) and the theoretical signals determined from MD simulations of model coordination modes using the 12-6 model (red lines).**

## EXAFS analysis of the Fe<sup>2+</sup>-polyGalA complex in an egg-box configuration with the modified 12-6 model

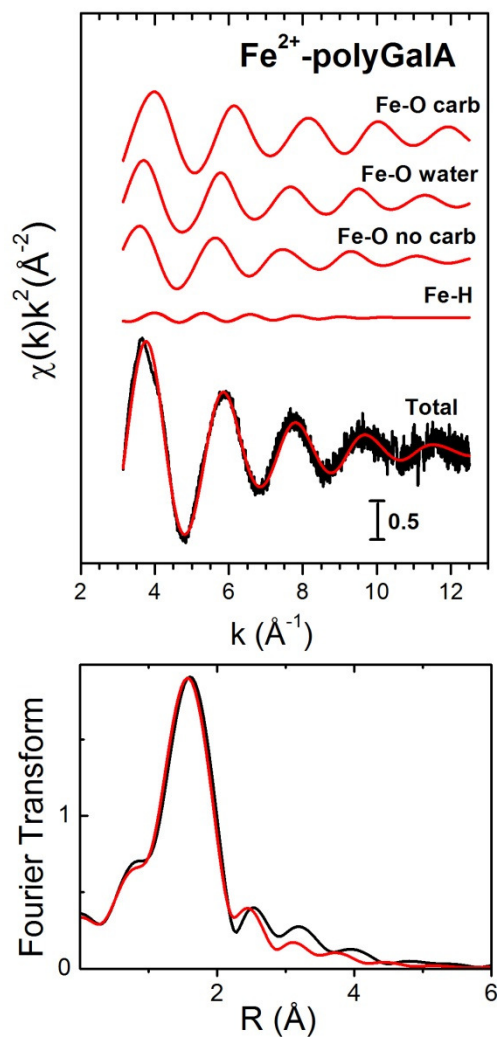


Figure S9. Fe K-edge EXAFS analysis of the Fe<sup>2+</sup>-polyGalA hydrogel in an "egg-box" configuration using the modified 12-6 model. Upper panel: Fe-O from carboxylate (Ocarb), water, non-carboxylate (no carb) oxygen atoms, and Fe-H two-body signals included in the fit, the total signal (red line) superimposed to the experimental one (black line). Lower panel: the fit in the Fourier transformed space.

## Conformations of polyGalA chains with the model coordination modes

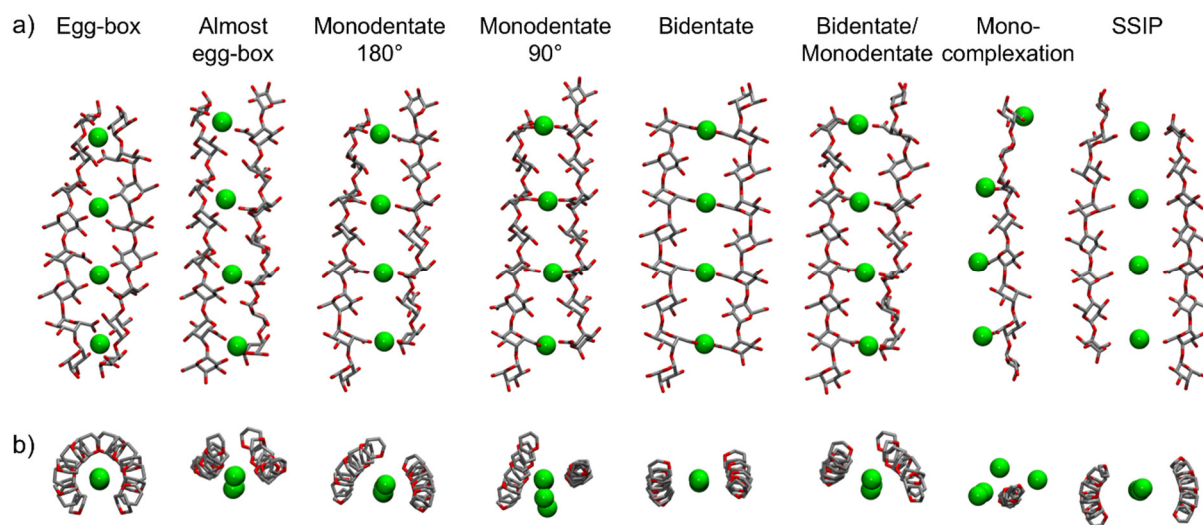


Figure S10. Time-averaged configurations formed by two octameric GalA chains in the antiparallel arrangement in the presence of four  $\text{Fe}^{2+}$  cations with the model coordination geometries considered in this study: (a) side view and (b) top view. Iron, oxygen, and carbon atoms are shown in green, red, and grey, respectively. For clarity, only heavy and ring atoms of GalA units are shown in (a) and (b), respectively.

## References

- 1 T. K. Sham, J. B. Hastings and M. L. Perlman, Structure and dynamic behavior of transition-metal ions in aqueous solution: an EXAFS study of electron-exchange reactions, *J. Am. Chem. Soc.*, 1980, **102**, 5904–5906.
- 2 B. S. Brunschwig, C. Creutz, D. H. Macartney, T.-K. Sham and N. Sutin, The role of inner-sphere configuration changes in electron-exchange reactions of metal complexes, *Faraday Discuss. Chem. Soc.*, 1982, **74**, 113–127.
- 3 M. Benfatto, J. A. Solera, J. García Ruiz and J. Chaboy, Double-channel excitation in the X-ray absorption spectrum of Fe<sup>3+</sup> water solutions, *Chem. Phys.*, 2002, **282**, 441–450.
- 4 P. D'Angelo and M. Benfatto, Effect of Multielectronic Configurations on the XAFS Analysis at the Fe K Edge, *J. Phys. Chem. A*, 2004, **108**, 4505–4514.
- 5 H. Ohtaki, T. Yamaguchi and M. Maeda, X-Ray Diffraction Studies of the Structures of Hydrated Divalent Transition-Metal Ions in Aqueous Solution, *Bull. Chem. Soc. Jpn.*, 1976, **49**, 701–708.
- 6 E. Kálmán, T. Radnai, G. Pálinkás, F. Hajdu and A. Vértes, Hydration of iron(II) ion in aqueous solutions, *Electrochim. Acta*, 1988, **33**, 1223–1228.
- 7 G. J. Herdman and G. W. Neilson, Ferrous Fe(II) hydration in a 1 molal heavy water solution of iron chloride, *J. Phys. Condens. Matter*, 1992, **4**, 649–653.
- 8 L. Dégrève and C. Quintale, The interfacial structure around ferric and ferrous ions in aqueous solution: the nature of the second hydration shell, *J. Electroanal. Chem.*, 1996, **409**, 25–31.
- 9 E. Guàrdia and J. A. Padró, Molecular dynamics simulation of ferrous and ferric ions in water, *Chem. Phys.*, 1990, **144**, 353–362.
- 10 C. S. Babu and C. Lim, Empirical Force Fields for Biologically Active Divalent Metal Cations in Water, *J. Phys. Chem. A*, 2006, **110**, 691–699.
- 11 F. Floris, M. Persico, A. Tani and J. Tomasi, Ab initio effective pair potentials for simulations of the liquid state, based on the polarizable continuum model of the solvent, *Chem. Phys. Lett.*, 1992, **199**, 518–524.
- 12 S. Amira, D. Spångberg, M. Probst and K. Hermansson, Molecular Dynamics Simulation of Fe<sup>2+</sup> (aq) and Fe<sup>3+</sup> (aq), *J. Phys. Chem. B*, 2004, **108**, 496–502.
- 13 L. A. Curtiss, J. W. Halley, J. Hautman and A. Rahman, Nonadditivity of ab initio pair potentials for molecular dynamics of multivalent transition metal ions in water, *J. Chem. Phys.*, 1987, **86**, 2319–2327.
- 14 P. Li and K. M. Merz, Taking into Account the Ion-Induced Dipole Interaction in the Nonbonded Model of Ions, *J. Chem. Theory Comput.*, 2014, **10**, 289–297.
- 15 Y. Jiang, H. Zhang and T. Tan, Rational Design of Methodology-Independent Metal Parameters Using a Nonbonded Dummy Model, *J. Chem. Theory Comput.*, 2016, **12**, 3250–3260.
- 16 D. Semrouni, W. C. Isley, C. Clavaguéra, J.-P. Dognon, C. J. Cramer and L. Gagliardi, Ab Initio Extension of the AMOEBA Polarizable Force Field to Fe<sup>2+</sup>, *J. Chem. Theory Comput.*, 2013, **9**, 3062–3071.
- 17 F. Duarte, P. Bauer, A. Barrozo, B. A. Amrein, M. Purg, J. Åqvist and S. C. L. Kamerlin, Force Field Independent Metal Parameters Using a Nonbonded Dummy Model, *J. Phys. Chem. B*, 2014, **118**, 4351–4362.
- 18 C. L. Kneifel, H. L. Friedman and M. D. Newton, Calculation of the Thermodynamic Solvent Isotope Effect for Ferrous and Ferric Ions in Water, *Z. Naturforsch. A*, 1989, **44**, 385–394.
- 19 T. Remsungnen and B. M. Rode, Molecular dynamics simulation of the hydration of transition metal ions: the role of non-additive effects in the hydration shells of Fe<sup>2+</sup> and Fe<sup>3+</sup> ions, *Chem. Phys. Lett.*, 2004, **385**, 491–497.
- 20 S. T. Moin, T. S. Hofer, A. B. Pribil, B. R. Randolf and B. M. Rode, A Quantum Mechanical Charge Field Molecular Dynamics Study of Fe<sup>2+</sup> and Fe<sup>3+</sup> Ions in Aqueous Solutions, *Inorg. Chem.*, 2010, **49**, 5101–5106.
- 21 T. Remsungnen and B. M. Rode, Dynamical properties of the water molecules in the hydration shells of Fe(II) and Fe(III) ions: ab initio QM/MM molecular dynamics simulations, *Chem. Phys. Lett.*, 2003, **367**, 586–592.
- 22 P. Li and K. M. Merz, Metal Ion Modeling Using Classical Mechanics, *Chem. Rev.*, 2017, **117**, 1564–1686.
- 23 S. L. Mayo, B. D. Olafson and W. A. Goddard, DREIDING: a generic force field for molecular simulations, *J. Phys. Chem.*, 1990, **94**, 8897–8909.
- 24 N. E. R. Zimmermann, B. Vorselaars, D. Quigley and B. Peters, Nucleation of NaCl from Aqueous Solution: Critical Sizes, Ion-Attachment Kinetics, and Rates, *J. Am. Chem. Soc.*, 2015, **137**, 13352–13361.
- 25 N. E. R. Zimmermann, M. K. Horton, A. Jain and M. Haranczyk, Assessing Local Structure Motifs Using Order Parameters for Motif Recognition, Interstitial Identification, and Diffusion Path Characterization, *Front. Mater.*, 2017, **4**, 34.
- 26 P. Mark and L. Nilsson, Structure and Dynamics of the TIP3P, SPC, and SPC/E Water Models at 298 K, *J. Phys. Chem. A*, 2001, **105**, 9954–9960.
- 27 H. J. C. Berendsen, J. P. M. Postma, W. F. van Gunsteren and J. Hermans, in *Intermolecular Forces*, ed. B. Pullman, Springer Netherlands, Dordrecht, 1981, vol. 14, pp. 331–342.
- 28 H. J. C. Berendsen, J. R. Grigera and T. P. Straatsma, The missing term in effective pair potentials, *J. Phys. Chem.*, 1987, **91**, 6269–6271.

- 29 H. W. Horn, W. C. Swope, J. W. Pitera, J. D. Madura, T. J. Dick, G. L. Hura and T. Head-Gordon, Development of an improved four-site water model for biomolecular simulations: TIP4P-Ew, *J. Chem. Phys.*, 2004, **120**, 9665–9678.
- 30 A. Assifaoui, A. Lerbret, H. T. D. Uyen, F. Neiers, O. Chambin, C. Loupiac and F. Cousin, Structural behaviour differences in low methoxy pectin solutions in the presence of divalent cations ( $\text{Ca}^{2+}$  and  $\text{Zn}^{2+}$ ): a process driven by the binding mechanism of the cation with the galacturonate unit, *Soft Matter*, 2015, **11**, 551–560.
- 31 W. L. Jorgensen, J. Chandrasekhar, J. D. Madura, R. W. Impey and M. L. Klein, Comparison of simple potential functions for simulating liquid water, *J. Chem. Phys.*, 1983, **79**, 926-935.
- 32 O. Guvench, S. N. Greene, G. Kamath, J. W. Brady, R. M. Venable, R. W. Pastor and A. D. Mackerell, Additive empirical force field for hexopyranose monosaccharides, *J. Comput. Chem.*, 2008, **29**, 2543–2564.
- 33 O. Guvench, E. Hatcher, R. M. Venable, R. W. Pastor and A. D. MacKerell, CHARMM Additive All-Atom Force Field for Glycosidic Linkages between Hexopyranoses, *J. Chem. Theory Comput.*, 2009, **5**, 2353–2370.
- 34 O. Guvench, S. S. Mallajosyula, E. P. Raman, E. Hatcher, K. Vanommeslaeghe, T. J. Foster, F. W. Jamison and A. D. MacKerell, CHARMM Additive All-Atom Force Field for Carbohydrate Derivatives and Its Utility in Polysaccharide and Carbohydrate–Protein Modeling, *J. Chem. Theory Comput.*, 2011, **7**, 3162–3180.